

https://doi.org/10.1070/QEL16831

In memory of Professor V.N. Bagratashvili (1947–2018)

Thermoplasmonic laser-induced backside wet etching of sapphire

M.Yu. Tsvetkov, N.V. Minaev, A.A. Akovantseva, P.S. Timashev,
A.E. Muslimov, V.M. Kanevskii

Abstract. **The technology of thermoplasmonic laser-induced backside wet etching is proposed to microstructure such solid and difficult-to-process materials as sapphire. In this technology, the laser absorbing medium is silver nanoparticles obtained from a precursor ($AgNO_3$) and providing significant laser radiation absorption due to the presence of plasmonic absorption with the formation of a substantially localised region with extremely high temperatures and pressures. This approach makes it possible to process sapphire both in the 'gentle' regime with the formation of nanometre structures and in the 'strong' regime to allow for the formation of 'deep' structures with etching rates up to several micrometers per pulse and high aspect ratio. The possibility of formation of periodic structures in sapphire in the above-threshold regime is shown.**

Keywords: *laser-induced backside wet etching, sapphire, thermoplasmonics, microstructuring, laser-induced periodic structures.*

1. Introduction

Synthetic sapphire (Al_2O_3) is increasingly used in micro- and optoelectronics, machine-building, instrument making and medicine. High optical uniformity and transparency of sapphire in a wide wavelength range, low residual stresses and radiation resistance are combined with good mechanical, thermo-oxidising, and dielectric properties which ensure the operation of sapphire products under high temperatures and pressures in contact with aggressive media [1, 2].

The formation of a microrelief on the sapphire surface is in high demand. Sapphire microstructuring can be used to produce substrates for light-emitting structures [3], anti-reflective coatings for radiation in the far-IR range [4] and other structures for microelectronics, photonics and microfluidics [5]. At the same time, sapphire processing (mechanical, ultrasonic, chemical) is a rather challenging task due to sapphire high hardness and chemical resistance. In recent years, in addition to traditional methods, laser technologies of sapphire processing, in particular, under the action of femtosecond laser pulses with subsequent chemical etching have been developed (see, for example, works [6–8]).

One of the promising methods of microstructuring of optically transparent materials is the method of laser-induced backside wet etching (LIBWE) (Fig. 1) [9]. In particular, this method has already been used for laser-induced sapphire etching (see, for example, [10–13]). In implementation of this process, high-intensity laser radiation (*1*) is focused on the rear surface of the transparent sample (*3*), which is located in the cell (*8*) filled with strongly absorbing liquid (*7*). In the focusing area (*4*), a whole series of processes occurs at the sample–liquid interface, including nonlinear radiation absorption, absorption on defects, photochemical, thermal, and hydrodynamic processes, formation of supercritical medium, cavitation, melting, evaporation, etc. [14–16]. These processes result in the formation of a substantially localised region at the liquid–solid interface with extremely high temperatures and pressures; in this case, strong temperature and pressure gradients thus formed contribute to the substance removal from the etching zone. The dominant LIBWE mecha-

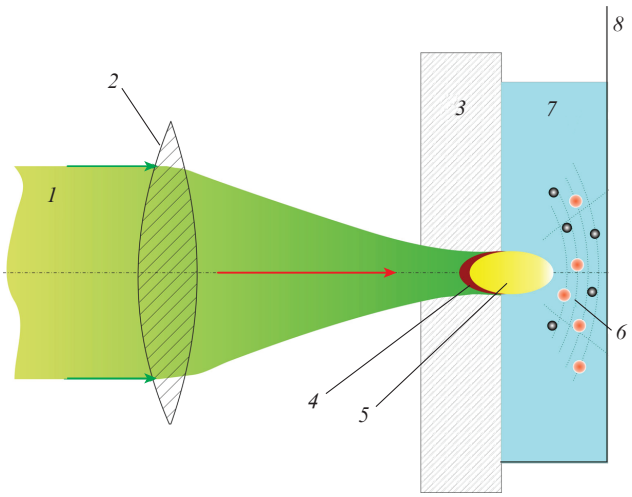

Figure 1. Block diagram of the LIBWE process:
(*1*) laser beam; (*2*) lens; (*3*) sapphire plate; (*4*) etching area; (*5*) plasma plume; (*6*) propagating shock waves and divergent nanoparticles; (*7*) absorbing liquid; (*8*) demountable cell.

M.Yu. Tsvetkov, N.V. Minaev, A.A. Akovantseva Institute of Photonic Technologies, Federal Scientific Research Centre 'Crystallography and Photonics', Russian Academy of Sciences, ul. Pionerskaya 2, 108840 Moscow, Troitsk, Russia; e-mail: mtsvet52@mail.ru;
P.S. Timashev Institute of Regenerative Medicine, I.M. Sechenov First Moscow State Medical University, ul. Trubetskaya 8, 119991 Moscow, Russia; Institute of Photonic Technologies, Federal Scientific Research Centre 'Crystallography and Photonics', Russian Academy of Sciences, ul. Pionerskaya 2, 108840 Moscow, Troitsk, Russia; N.N. Semenov Institute of Chemical Physics, Russian Academy of Sciences, ul. Kosygina 4, 119991 Moscow, Russia;
e-mail: timashev.peter@gmail.com;
A.E. Muslimov, V.M. Kanevskii Institute of Crystallography, Federal Scientific Research Centre 'Crystallography and Photonics', Russian Academy of Sciences, Leninsky prosp. 59, 119333 Moscow, Russia;
e-mail: amuslimov@mail.ru, kanev@crys.ras.ru

Received 2 October 2018; revision received 19 October 2018
Kvantovaya Elektronika **49** (2) 133–140 (2019)
Translated by M.A. Monastyrskiy

nisms, substance removal rate and parameters of the microstructures formed are determined by the substance type, liquid composition and parameters of pulsed laser radiation.

And here, from our viewpoint, an approach based on the use of nanoparticles as an absorbing medium in which the occurrence of plasmon resonance is possible could make a significant contribution to the development of LIBWE microstructuring (see our work [17–19]). When laser radiation affects nanoparticles in metal, the electric field of a light wave excites collective oscillations of conduction electrons, which are called surface plasmons [20]. At certain optical frequencies, such oscillations are excited in resonance with significant charge shifts and the generation of local electromagnetic fields. For a considerable period of time, the resulting plasmon absorption and subsequent temperature rise of nanoparticles were considered as a not so significant effect, and only recently attention has been paid to the fact that resonant light absorption makes metallic nanoparticles ideal heat sources and provides unprecedented ways of implementing thermally induced phenomena localised in the zone of laser radiation interaction with a plasmon medium [21, 22].

This work shows the possibility of using thermoplasmonic LIBWE (TP-LIBWE) with $AgNO_3$ as a precursor of silver nanoparticles for laser micromachining of sapphire. The contribution to microstructuring of sapphire in the processes occurring under conditions typical of supercritical media is discussed. Various types of the thus formed structures are demonstrated. It is shown that in this process, silver nanoparticles (AgNP) are formed as a result of precursor recovery.

2. Experiment

A schematic of the experiment and corresponding installation are described in our work [23, 24] dedicated to the study of various regimes of optical glass etching. As samples, we used two-side-polished basic-oriented sapphire substrates with a diameter of 50.8 mm and a thickness of ~0.45 mm, obtained from the sapphire single crystals grown by the Kyropoulos–Musatov method [25]. The substrate blanks were cut out with diamond saws and crowns; abrasive powders or tools based on diamond and boron carbide were used for their grinding and mechanical polishing. Two-sided chemical-mechanical polishing of substrates was carried out on polyurethane lapping using a silicasol-based suspension. All operations were completed by washing the blanks and measuring the monitored parameters. In particular, the relief and surface roughness after machining were measured with a mechanical profilometer, while those obtained after chemical-mechanical polishing – using atomic-force microscopy and X-ray scattering.

For etching the samples, we used radiation from a TECH-527 Basic diode-pumped solid-state laser (Laser Compact, Russia) with a wavelength of 527 nm, a laser pulse duration of τ = 5 ns, a maximum pulse energy of E = 250 μJ, a linear polarisation of 100:1 and a divergence of less than 3 mrad. The plate to be etched was installed as the front wall of a dismountable cell filled with a working fluid – a saturated 5-molar aqueous solution of silver nitrate ($AgNO_3$), laser-induced decomposition of which ensures the appearance of strongly absorbing silver nanoparticles and thermoplasmonic effect in the system. The cell with the sample and working fluid was placed on an 8MT167-100 three-axis translation stage (Standa) with positioning accuracy no worse than 2 μm. To focus radiation on the rear surface of the plate, a 10× LMH-10X-532 lens (Thorlabs) with NA = 0.25 was used. A laser beam with a Gaussian intensity distribution profile and given energy and geometric parameters (see below) was directed to the lens using a dichroic mirror and focused on the interface between the liquid and the transparent surface of a sapphire sample. Visual express control of craters and channels formed in the process of TP-LIBWE experiments was carried out on the basis of images obtained through a dichroic mirror using an EXCCD00300KMA USB camera (ToupTek) when illuminated with white light from the illuminator. This enabled precise alignment of the sample, and also the possibility of observing the surface during the etching process.

Experiments on laser-plasmon microstructuring of sapphire samples were performed at a pulse repetition rate of 1 kHz and laser radiation energies up to 25 μJ per pulse. The sample was irradiated both with focused (rear plane of the plate was located in the region of the laser beam waist) and defocused (the beam waist was shifted into the absorbing liquid for a distance up to 20 μm) beams. Focusing parameters of the Gaussian laser beam are determined by the beam diameter in front of the focusing lens, and also by the lens parameters [26]. In our case, the beam diameter was varied from 1.4 to 4 mm. This made it possible to form areas with the following parameters near the focus at the interface between the sample and absorbing liquid: diameter of the laser beam waist 3.4–9.6 μm (at the 1/e level), waist length from ~30 to ~300 μm. When the focus was shifted, the beam diameter in the etching region increased up to 20 μm. Under the experimental conditions, the energy density Φ reached 30 J cm^{-2}.

Experiments on the formation of craters were performed by varying Φ and N (the number of laser pulses) and also by shifting the laser beam waist relative to the rear surface of the plate. The channels were formed at a laser beam scan rate of 8–140 μm s^{-1} on the sample surface. The geometry, shape and surface characteristics of the microstructures formed in the samples were studied using optical scanning electron microscopy (SEM) and atomic force microscopy (AFM). Optical images of laser structures at various energy densities of laser pulses were obtained using an HRM-300 optical microscope (Huvitz, Korea) equipped with functions of three-dimensional visualisation of the surface topography and a Contour GT-K optical profilometer (Bruker). SEM images were obtained using Phenom ProX and Jeol JCM-6000 Plus scanning electron microscopes at 10 kV accelerating voltages. An INTEGRA-Terma scanning probe nanolaboratory (NT-MDT, Russia) was used to obtain AFM images using Veeco RTESP silicon cantilevers with a resonant frequency of 300–360 kHz and a curvature radius of the cantilever tip less than 5 nm. Scanning was performed in a semi-contact regime in the air at constant amplitude (topography). The working fluid extinction spectra were recorded using a Cary 50 spectrometer (Varian).

3. Results of the experiment

In the implementation of the TP-LIBWE process, craters and channels were formed on the sapphire plate surface, both when the beam was focused on the interface between the sample and absorbing liquid and when the focus was shifted relative to the interface into the liquid medium. The characteristics of the thus formed structures were investigated as function of the laser energy density, number of irradiation pulses, and/or scan rate. The dependence of the crater etching depth

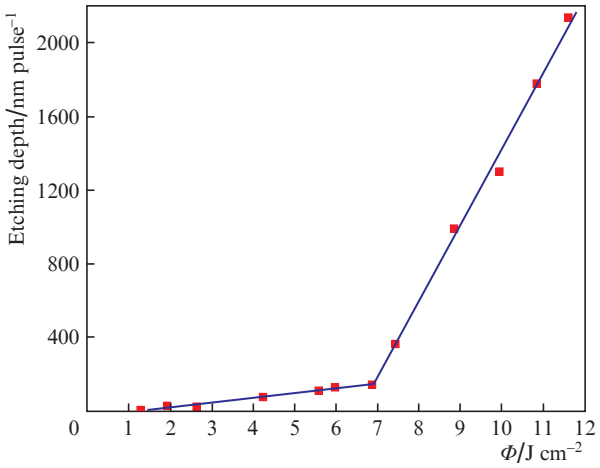

Figure 2. Dependence of the crater etching depth per pulse on the energy density of laser radiation.

on the laser energy density under irradiation by a sequence of 200 pulses was used to determine the TP-LIBWE sapphire threshold Φ_{thr}, which in our case amounted to ~ 1.5 J cm^{-2} (Fig. 2).

It was found that, as the density of laser radiation energy is varied, there occur significant changes in morphology and surface etching rate, which makes it possible to distinguish two processing regimes similar to the regimes of sapphire ablation by ultrashort pulses, namely 'gentle' ($\Phi \leqslant 7$ J cm^{-2}) and 'strong' [27] regimes.

3.1. Etching near the threshold and formation of laser-induced periodic ring surface structures

Quite an interesting picture was observed when channels were formed in sapphire plates in the case of minimal excess of the structuring threshold. Figures 3a and 3b present the AFM images of the channels with a width of ~ 6 μm, obtained as a result of scanning a Gaussian laser beam with 10 passes. Initially, with a minimum threshold excess, removal of the impaired surface layer of the substance occurs [28]. In our case, the depth of such a layer reaches 15 nm. Further on, as the energy density increases, gradual formation of the laser-induced periodic surface structures (LIPSS's) starts in the central part of the channel.

In our case, the LIPSS's have a concentric structure. They are formed at laser radiation intensities lying in a fairly narrow range of energy densities (1.5–2 J cm^{-2}). The LIPSS period is 0.4–0.7 μm which is close enough to the incident laser radiation wavelength; in this case, the heterogeneity of the structure and the sample surface can be manifested in the process of their formation. Similar periodic structures were obtained in the formation of craters in sapphire as a result of sample irradiation with both focused and defocused laser beams (Fig. 3c).

'Classical' LIPSS's (see, for example, review [29] and references therein) which are usually obtained under irradiation by short (pico- and femtosecond) laser pulses are oriented perpendicular or parallel to the polarisation direction of laser radiation. They emerge under the action of laser pulses of various durations and in different materials. In particular, similar structures were formed in fused quartz under irradiation with pulses of 600 fs duration in the LIBWE geometry [30].

At the same time, in a number of works, concentric LIPSS's or, as they are also called, laser-induced periodic annular surface structures (LIPASS's), were observed (see, for example, [31–35]), similar to those obtained by us. We assume that the formation of such structures is most likely affected by laser radiation interference arising from the interaction of radiation with matter [33] (see Section 4.2) in combination with possible processes of mass transfer and self-organisation in a thin molten surface layer at the interface between the sapphire and absorbing medium [31] (see Section 4.3).

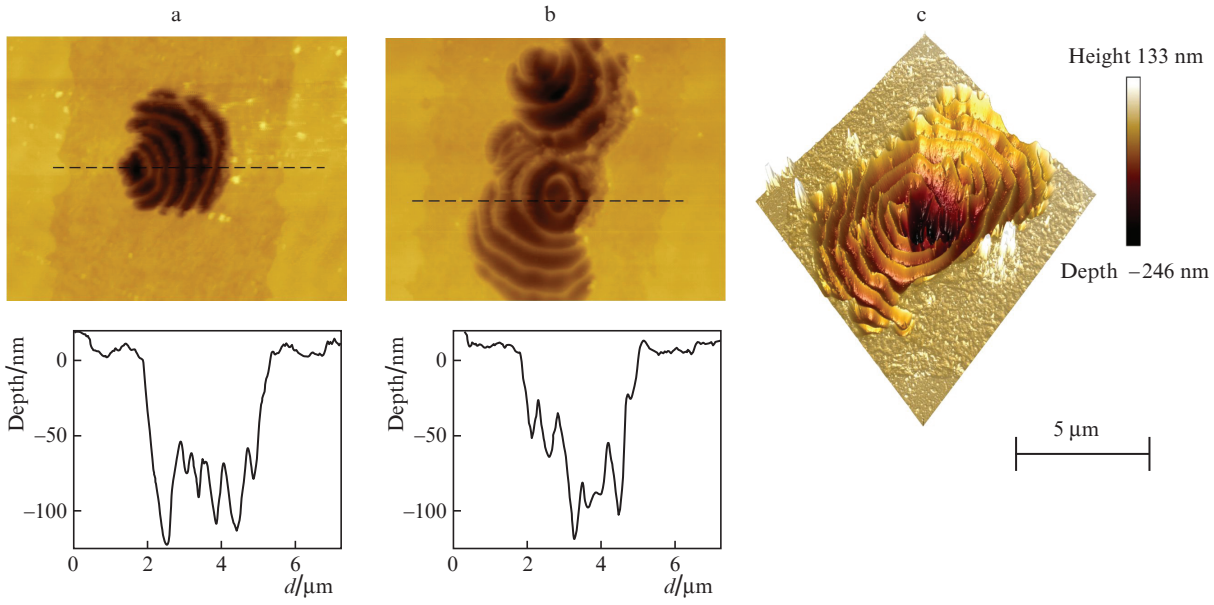

Figure 3. (a, b) AFM images and corresponding microstructure profiles on sapphire, obtained with the laser energy density increase and (c) 3D AFM image of the crater.

3.2. 'Gentle' and 'strong' etching regimes using nanosecond laser radiation

The etching geometry is determined by the parameters of initial beam and focusing optics [26, 36]; in particular, the focused beam diameter satisfies the relation

$$w = \left(\frac{4\lambda}{\pi}\right)\left(\frac{F}{D}\right),$$

while the waist length appears as

$$b = \left(\frac{8\lambda}{\pi}\right)\left(\frac{F}{D}\right)^2,$$

where λ is the laser radiation wavelength, F is the lens focal length, and D is the initial size of the laser beam.

At the initial stage, craters and channels with the geometry determined by the Gaussian profile of the laser beam are formed in the area of 'gentle' etching (Fig. 4). The etching rates in this area constitute several tens of nanometers per pulse. When the threshold turns out somewhat exceeded, the diameter d_0 of the formed crater (channel) only slightly exceeds the diameter w of the focused beam. As the energy density and/or the number of laser pulses increase, the crater (channel) depth gradually increases with a simultaneous moderate (up to 1.5 times) increase in diameter.

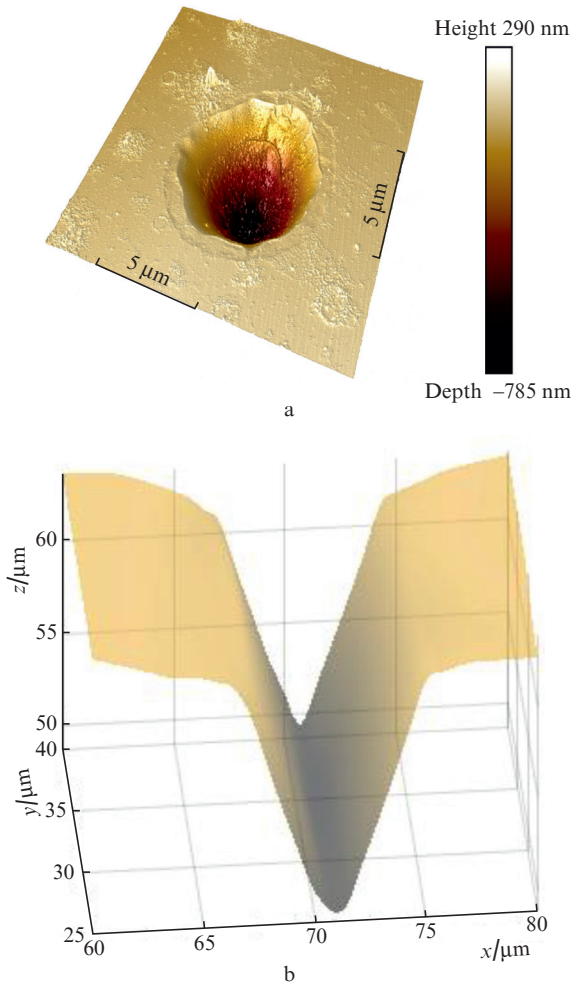

Figure 4. 3D images of (a) the crater and (b) channel in the 'gentle' etching area, obtained using AFM and optical microscope, respectively.

In transition to the 'strong' etching area ($\Phi \gtrsim 7$ J cm^{-2}), an increase in Φ is accompanied by a rapid increase in the etching depth per pulse, which reaches and even exceeds ~ 1 μm per pulse. In this case, smooth craters and channels up to 200 μm in depth, with a fairly large (over 10) aspect ratio, are formed.

Analysing the value of the etching depth per pulse at a fixed focus in the 'strong' etching regime, several areas can be identified. Those areas are schematically shown in Fig. 5 (the dependence presented was obtained at the origin of the energy density region of 'strong' etching at $\Phi \sim 7.2$ J cm^{-2} and $w \sim 7$ μm). It should be noted that particular values of the etching depth may vary greatly depending on the energy density of laser radiation and beam parameters.

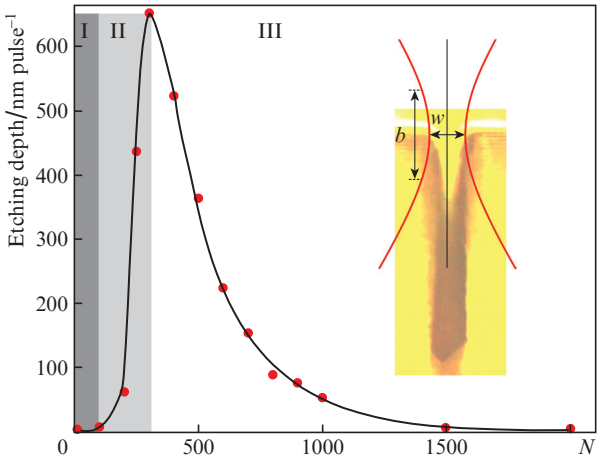

Figure 5. Typical dependence of the etching depth per pulse on the number of pulses N at an immobile focus for the 'strong' etching regime. The inset shows the mutual position of the laser beam waist and the formed channel.

At the initial stage of etching (region I), an incubation period is observed, associated with the formation of AgNP from a precursor and the appearance of an absorbing layer (see Section 4.1). At this stage, with exposure to several tens of pulses, absorbing nanoparticles emerge. There is virtually no etching in this case.

As the medium absorption (region II) grows, the etching rate reaches a level determined by the energy density of laser radiation (see Fig. 2). The Gaussian distribution of the laser radiation intensity at the beam centre provides a 'strong' etching regime, and closer to the periphery (crater walls) – a 'gentler' regime, which enables the formation of a smooth surface of the crater's side walls.

At large depths of craters (channels) in region III, a decrease in the etching rate is observed due to the fact that the laser beam waist is shifted from the region of the most intense etching (note that in this work we used the regimes without scanning the beam in depth). This changes the etching geometry, and the walls of craters (channels) become almost vertical (Figs 6a and 6b), which is caused by the beam expansion in the etching region; the beam profile becomes smoother, while the intensity decreases [37]. Eventually, the laser energy density in the etching area drops below the threshold, and the etching process gradually terminates.

Preliminary experiments using a telecentric F-Theta lens (Ronar-Smith, Singapore) with a focal length of 110 mm have shown that the dependence of the etching depth on the num-

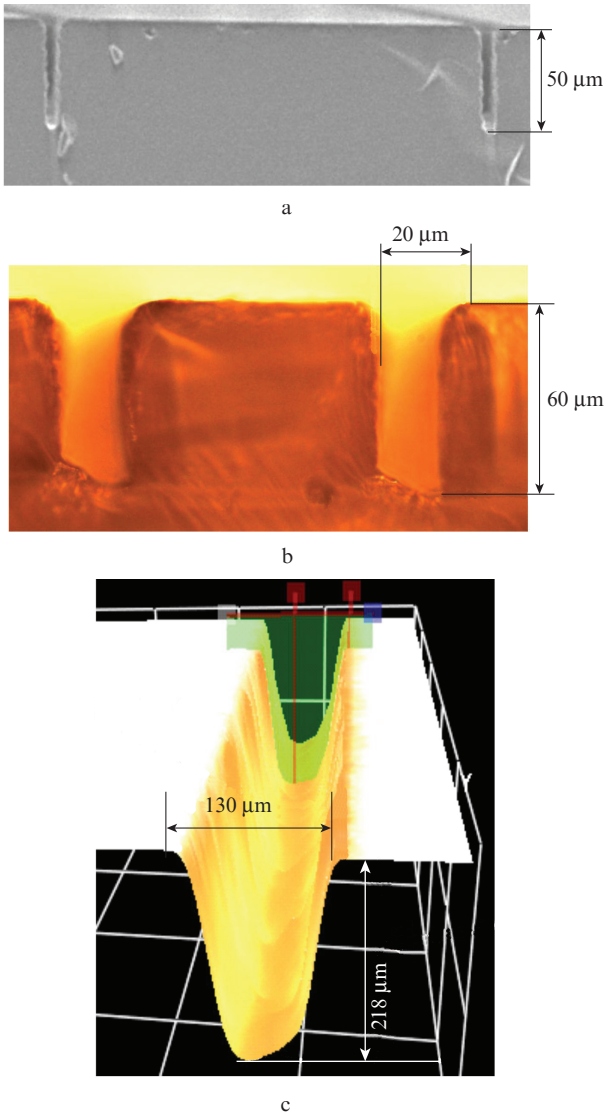

Figure 6. (a) SEM and (b) optical microscope images of channels formed in the 'strong' regime and (c) 3D image of the channel formed by scanning the laser beam in the cross section.

ber of pulses for a smoother and longer beam caustic is virtually linear.

For the formation of craters with diameters up to $(2-3)d_0$, etching regimes under defocused laser beam conditions were used. To obtain wider channels, the laser beam passed along them several times with a slight offset in the perpendicular direction (Fig. 6c).

With a significant increase in the energy density, photomechanical processes [38] start to play an important role, causing the formation of cracks and splits, which ultimately leads to the formation of structures of inadequate quality and their destruction.

4. Discussion

When focused laser radiation is incident on the rear surface of a sample placed in contact with a highly absorbing liquid, a substantially localised region with extremely high temperatures and pressures is formed (see Fig. 1) [9, 19], which is accompanied by numerous physico-chemical processes resulting in laser-induced etching of the sample material. With the appropriate choice of the laser beam trajectories (here we confine ourselves to the method of direct laser writing) and careful selection of the process parameters, it is possible to perform microstructuring of the sample surface in accordance with the specified design.

The physics and chemistry of LIBWE is determined by thermodynamics of the processes of laser radiation interaction with media, passing through various phase states, and are largely similar to the ablation of nanoparticles in liquid [39, 40].

The main stages of TP-LIBWE include the laser radiation absorption by a solution of a plasmonic precursor, photothermal processes of the formation of a highly localised medium with plasmonic nanoparticles, ultrafast heating of the solution and dielectric to extremely high temperatures, the substance transition to a supercritical state, laser-induced release of the sample material with the formation of microstructures on its surface. Removal of the sample material is accompanied by the hydrodynamic processes in which the substance is removed from the etching zone and gradually cools down; as a result, nanoparticles and clusters of them are formed, remaining in the bulk of liquid and on the surface of the material being processed.

4.1. Formation of a plasmonic medium

When an aqueous solution of silver nitrate interacts with intense laser radiation, the mechanism of reducing the precursor to silver nanoparticles is triggered. Laser radiation initiates the formation of active intermediates in the solution, which leads to the formation of silver atoms Ag [41, 42] with a gradual transition from individual atoms to silver nanoparticles [43, 44].

At the laser irradiation onset, an 'incubation' period is observed, when the process of laser-induced etching does not virtually occur and active reducing of silver nanoparticles from the precursor takes place. Next, a peak of plasmonic absorption is formed with a maximum near $\lambda \approx 430$ nm and a wide long-wavelength wing (see Fig. 5c in work [17]), which indicates the appearance of spherical and quasi-spherical silver nanoparticles with average diameters of ~ 50 nm in the working fluid and a significant spread in size [45].

As the size of nanoparticles increases, the plasmonic absorption peak shifts to the long-wavelength region. In this case, the first 'seed' pulses of incident laser radiation form the centres of additional 'plasmon' absorption; the process develops in an avalanche-like manner and after while comes to a stationary regime. Thus, a region with high concentration of 'plasmon' nanoparticles is formed at the interface with the sample surface being processed. Thus, a significant amount of nanoparticles is deposited on the surface of the processed sapphire plate and in the pores of the formed microstructures.

To remove the nanoparticles after the process termination, we used nitric acid mixed with water in a ratio of 1 : 3. To ensure the access of this mixture to pores with a large aspect ratio, processing in an ultrasonic bath was employed, after which the samples were washed in deionized water.

4.2. LIBWE mechanisms

Laser radiation is almost completely absorbed in a thin layer of the medium containing 'plasmon' nanoparticles at the interface with the sapphire surface. Such a highly localised heat source with a large energy release at the solid–liquid

interface initiates thermal, thermochemical and hydrodynamic processes that are similar to the processes accompanying the ablation of the sample material in a liquid medium [39, 40].

Mechanisms similar to the case of hydrocarbon LIBWE are implemented, when the decomposition of an organic liquid results in the formation of a carbon layer that strongly absorbs laser radiation and provides etching rates from units to hundreds of nanometers per pulse [9, 46–48]. The advantage of TP-LIBWE is that the laser radiation wavelength falls into the plasmon resonance band of nanoparticles and an absorbing medium is formed, providing the etching rates that are at least an order of magnitude larger under the same experimental conditions.

Of interest are the mechanisms leading to the formation of LIPASS's in the above-threshold regime. Like any other material, sapphire has certain defects that serve as sources of heat generation and spherical scattering waves [49]. In the formation of channels, similar 'seeds' arise in the central part of the channel, i.e., in the region where the energy density of laser radiation attains its maximum. As the energy density Φ increases, the number of those 'seeds' gradually increases (see Figs 3a and 3b), and the process of laser-induced substance etching with the formation of craters starts [24, 39]. Point 'sources' of scattering are replaced by the scattering surfaces of craters. In this case, the crater geometry determines the concentric pattern of laser radiation interference. A variant of such a pattern formation for the case of femtosecond laser ablation is considered in [33].

4.3. Thermodynamics of etching processes

Exact description of the TP-LIBWE mechanisms is rather complicated. In this case, numerous physical processes, the nature and efficiency of which depend on the laser radiation parameters, may simultaneously occur at different points of the laser spot. As an analogy, we may consider laser ablation processes in a liquid medium [39, 40]. As a rule, methods of thermodynamics [50, 51] and molecular dynamics [52] are used to describe these processes.

In general case, laser radiation absorption results in the formation of hot carriers (electrons or electron–hole pairs), which, as a result of phonon emission, heat initial cold ions to the equilibrium state for 10^{-12}–10^{-11} s [38]. This time scale is essential since it establishes an interface between the predominantly thermal and predominantly non-thermal ways of laser radiation interaction with matter, separating the ranges of 'long' and 'short' pulses [38]. In the case of nanosecond pulses, the equilibrium between electrons and phonons prevails at the heating stage termination, and phase changes can be considered as a thermal process that includes quasi-equilibrium thermodynamic states. In this case, temporal parameters of the process of plasmon laser-induced etching are determined by the interaction of the region with a high concentration of 'plasmon' nanoparticles as a whole with media – the surface of the processed dielectric.

The literature discusses three types of thermal processes that can lead to the separation of substance at a solid–liquid interface under similar conditions: normal evaporation, normal boiling and 'explosive boiling' [39, 53]. In this case, normal boiling occurs in the case of long (hundreds of microseconds or more) laser pulses and is unable to develop in the nanosecond range of durations [53].

At moderate radiation intensities, the mechanism of normal evaporation is realised [54], at which atoms and molecules are removed from the solid body surface. Thus, in the case of pulsed laser heating, as opposed to slow heating, this regime can be maintained at sufficiently high temperatures and pressures (superheat regime) [53, 55]. We assume that in our case it corresponds to the 'gentle' etching regime.

Under the above-threshold conditions, in a rather narrow range of incident laser energy densities (1.5–2 J cm^{-2}), we observed the formation of periodic structures (LIPASS's) on the sapphire surface. It is worth noting that during the formation of such structures, along with the interference of light waves (see Section 4.2), possible is the influence of mass transfer and self-organisation processes arising on the surface of the processed material within a thin layer at the interface between the material boundary and absorbing medium under the action of interfering laser radiation (see, as example, [56, 57]). The estimates given in these works show that thermocapillary flows may occur within the molten surface layer under the action of periodically distributed laser energy, which leads to the molten material redistribution on the surface under processing. These processes cause the formation of characteristic periodic LIPASS patterns (period of structures is $\Lambda \sim \lambda$) which becomes 'frozen' at the end of the process of nanosecond laser irradiation.

With an increase in the energy density of laser radiation (in our case, at $\Phi \gtrsim 7$ J cm^{-2}) due to laser radiation absorption by 'plasmonic' nanoparticles, their heating, and subsequent heat transfer to the surrounding medium, the microvolume of the absorbing liquid and near-surface area of the sample is rapidly heated, which is accompanied by the formation of supercritical water (critical parameters for water are T_c = 647.1 K, P_c = 22.1 MPa) [58, 59], melting, boiling, and evaporation of the sample material. The substance is abruptly transferred to the near- and supercritical states (for sapphire, T_c = 5335 K [60]). A transition from normal evaporation to 'explosive boiling' or, in other words, a 'phase explosion' occurs [39, 61].

From our point of view, these processes correspond to the 'strong' etching regime. In this case, the laser-exposed medium is transferred to the state of supercritical fluid; temperatures may reach several thousand kelvins, while pressures may attain several gigapascals [62]. It should be noted here that supercritical water can play a significant role in the process of laser etching. It is known that, unlike 'ordinary' water, it is highly reactive [63, 64], and the time of energy exchange between the medium components can be significantly reduced [65].

The study of these and related processes (for example, the thickness of the absorbing layer of plasmon nanoparticles) requires both estimating the temperature and pressure of the medium under extreme conditions, and performing measurements with high temporal resolution directly in the course of experiment using, for example, the methods of shadow high-speed imaging [66], as we plan for the future.

Due to the presence of large temperature and pressure gradients in the laser impact region, the substance in the plasma state starts to expand. On the time scales of 10^{-10}–10^{-7} s, a 'plasma plume' is formed, which contributes to the substance removal from the etching zone [39]. At the laser pulse termination, the pressure and temperature of the medium fall, and hydrodynamic processes (formation and collapse of bubbles, shock waves) become predominantly influent, which lead to

the sample material removal from the etching zone. The nanoparticles and nanoclusters nucleate and form [39].

5. Prospects of the method

The developed approach provides a possibility of forming various functional microstructures for numerous applications. As an example, Fig. 7 shows a matrix manufactured to form the prototypes of structured bio-substrates.

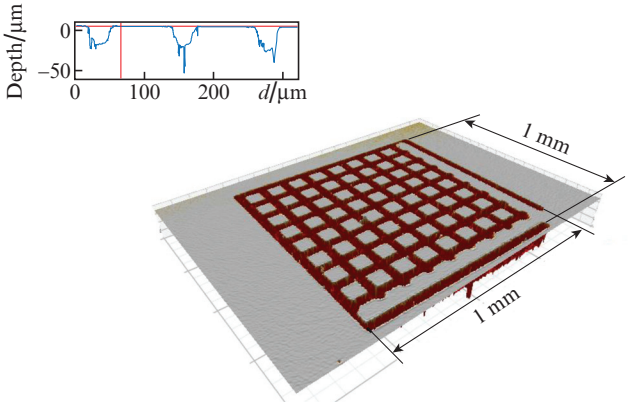

Figure 7. 3D image of a 1 × 1 mm grid of channels formed on a sapphire plate (the inset shows a profile example).

The LIBWE method enables the formation of reproducible structures with variable parameters and a roughness on the scale of few microns, which corresponds to the structures affecting the functional activity of cells [67]. The structures formed on artificial sapphire will have significant advantages, and primarily stability stipulated by the possibility of multiple appliance and washing, good affinity to cells and high optical transparency. The development of 3D substrates for cell cultivation and analysis of their proliferation, differentiation, and the formation of intercellular contacts will in the future allow the creation of models of various tissues in the Lab-on-a-Chip system [68].

The development of 2D structures requires careful selection of focusing conditions and the use in laser drawing of many laser beam passes with various speeds and scanning geometries [28, 69]. This offers a possibility of forming structures with different geometries and surface quality (waviness, roughness), which will allow, as example, investigation on the adhesion of cellular structures in solving certain biomedical problems (formation of microchips). For this purpose, it is assumed to use various regimes of forming microstructures in the shape of channels, channel systems and/or platforms.

Thus, the present work has demonstrated the possibilities of using the thermoplasmonic LIBWE method for microstructuring of such a promising, but at the same time solid and difficult-to-process optical material as sapphire. Various regimes of sapphire etching have been revealed: the regime of gentle etching with rates up to several tens of nanometers per pulse, ensuring the formation of structures with a small aspect ratio, but high surface quality, and the 'strong regime' with significantly higher etching rates (microns per pulse), providing the formation of channels with a high aspect ratio and structures. A technology has been developed for manufacturing several basic structures, on the basis of which the possibilities for various applications of this technology are considered.

Acknowledgements. This work was supported by the Russian Foundation for Basic Research (Grant No. 18-02-00420 A) in part of the design of the laser microstructuring facility and in part of the studies on sapphire etching processes at supercritical temperatures (Grant Nos 18-29-06056 MK; 16-29-11763 ofi-m). This work was also supported by the Russian Science Foundation (Grant No. 14-33-00017-P0) in part of the development of equipment to operate with supercritical temperatures and pressures and by the Federal Agency for Scientific Organisations (Agreement No. 007-GZ/Ch3363/26) in part of the development of microstructuring technologies. The authors thank A.P. Sviridov for helpful discussions, D.A. Fokin and A.G. Shubny for their assistance in conducting measurements.

References

1. Dobrovinskaya E.R., Lytvynov L.A., Pishchik V.V. *Sapphire. Material, Manufacturing, Applications* (New York: Springer, 2009).
2. *Sapphire: Structure, Technology, and Application*. Ed. by I. Tartaglia (New York: Nova Sci. Publ., 2013).
3. Kuna L., Haase A., Reil F., Sommer C., Krenn J.R., Hartmann P., Pachler P., Tasch S., Wenzl F.P. *IEEE J. Sel. Top. Quantum Electron.*, **15**, 1250 (2009).
4. Matsumura T., Young K., Wen Q., Hanany S., Ishino H., Inoue Y., Hazumi M., Koch J., Suttman O., Schütz V. *Appl. Opt.*, **55**, 3502 (2016).
5. Teplova T.B., Samerkhanova A.S. *Gornyi informatsionno-analiticheskii byulleten' No. 10* (Mining Information and Analytical Bulletin No. 10) (M.: Gornaya kniga, 2006) p. 339.
6. Hörstmann-Jungemann M., Gottman J., Keggenhoff M. *J. Laser Micro/Nanoeng.*, **5**, 145 (2010).
7. Li Q.-K., Yu Y.-H., Wang L., Cao X.-W., Liu X.-Q., Sun Y.-L., Chen Q.-D., Duan J.-A., Sun H.-B. *IEEE Photon. Techn. Lett.*, **28**, 1290 (2016).
8. Liu M., Hu Y., Sun X., Wang C., Zhou J., Dong X., Yin K., Chu D., Duan J. *Appl. Phys. A*, **123**, 99 (2017).
9. Zimmer K., Ehrhardt M., Böhme R. *Laser-Induced Backside Wet Etching: Processes, Results, and Applications*, in: *Laser Ablation* in *Liquids: Principles and Applications in the Preparation of Nanomaterials*. Ed. G. Yang (Singapore: Pan Stanford Publ., 2012).
10. Dolgaev S.I., Lyalin A.A., Simakin A.V., Shafeev G.A. *Appl. Surf. Sci.*, **96–98**, 491 (1996).
11. Dolgaev S.I., Karasev M.E., Kulevsky L.A., Simakin A.V., Shafeev G.A. *Quantum Electron.*, **31**, 593 (2001) [*Kvantovaya Elektron.*, **31**, 593 (2001)].
12. Ding X., Sato T., Kawaguchi Y., Niino H. *Jpn. J. Appl. Phys.*, **42**, L176 (2003).
13. Pissadakis S., Böhme R., Zimmer K. *Opt. Express*, **15**, 1428 (2007).
14. Niino H., Yasui Y., Ding X., Narazaki A., Sato T., Kawaguchi Y., Yabe A. *J. Photochem. Photobiol. A: Chem.*, **158**, 179 (2003).
15. Vass C., Budai J., Schay Z., Hopp B. *J. Laser Micro/Nanoeng.*, **5**, 43 (2010).
16. Zimmer K., Böhme R., Ehrhardt M., Rauschenbach B. *Appl. Phys. A*, **101**, 405 (2010).
17. Tsvetkov M.Yu., Yusupov V.I., Minaev N.V., Timashev P.S., Golant K.M., Bagratashvili V.N. *Las. Phys. Lett.*, **13**, 106001 (2016).
18. Tsvetkov M.Yu., Yusupov V.I., Timashev P.S., Golant K.M., Minaev N.V., Bagratashvili V.N. *Nanotechnol. Russ.*, **12**, 86 (2017) [*Ross. Nanotekh.*, **6**, 69 (2017)].
19. Tsvetkov M.Yu., Minaev N.V., Akovantseva A.A., Pudovkina G.I., Timashev P.S., Tsypina S.I., Yusupov V.I., Muslimov A.E., Butashin A.V., Kanevsky V.M., Bagratashvili V.N. *Russ. J. Phys. Chem. B*, **11**, 1288 (2017) [*Sverkhkrit. Flyuidy: Teor. Prakt.*, **12**, 68 (2017)].
20. Kreibig U., Vollmer M. *Optical Properties of Metal Clusters* (New York: Springer-Verlag, 1995).
21. Govorov A.O., Richardson H.H. *Nanotoday*, **2**, 30 (2007).

22. Baffou G., Quidant R. *Laser Photon. Rev.*, **7**, 171 (2013).
23. Tsvetkov M.Yu., Yusupov V.I., Minaev N.V., Akovantseva A.A., Timashev P.S., Golant K.M., Chichkov B.N., Bagratashvili V.N. *Opt. Las. Technol.*, **88**, 17 (2017).
24. Tsvetkov M.Yu., Yusupov V.I., Timashev P.S., Golant K.M., Minaev N.V., Tsypina S.I., Bagratashvili V.N. *Russ. J. Phys. Chem B.*, **11**, 1061 (2017) [*Sverkhkrit. Flyuidy: Teor. Prakt.*, **11**, 14 (2016)].
25. Muslimov A.E., Asadchikov V.E., Butashin A.V., Vlasov V.P., Deryabin A.N., Roshchin B.S., Sul'yanov S.N., Kanevsky V.M. *Crystallogr. Rep*., **61**, 730 (2016) [*Kristallograf.*, **61**, 703 (2016)].
26. Siegman A.E. *Lasers* (Mill Valley, Cal: Univ. Sci. Books, 1986).
27. Ashkenasi D., Stoian R., Rosenfeld A. *Appl. Surf. Sci.*, **154–155**, 40 (2000).
28. Wei X., Xie X.Z., Hu W., Huang J.F. *Intern. J. Opt.*, Article ID 238367 (2012); doi:10.1155/2012/238367 (2012).
29. Buividas R., Mikutis M., Juodkazis S. *Progr. Quantum Electron.*, **38**, 119 (2014).
30. Böhme R., Vass C., Hopp B., Zimmer K. *Nanotechnol.*, **19**, 495301 (2008).
31. Ma F., Yang J., Zhu X., Liang C., Wang H. *Appl. Surf. Sci.*, **256**, 3653 (2010).
32. Nayak B.K., Gupta M.C. *Opt. Las. Eng.*, **48**, 966 (2010).
33. Liu Y., Brelet Y., He Z., Yu L., Forestier B., Deng Y., Jiang H., Houard A. *Appl. Phys. Lett.*, **102**, 251103 (2013).
34. Sun W., Qi H., Fang Z., Yu Z., Liu Y., Yi K., Shao J. *Opt. Express*, **22**, 2948 (2014).
35. Sun W., Qi H., Fang Z., Yu Z., Yi K., Shao J. *App. Surf. Sci.*, **309**, 79 (2014).
36. http://assets.newport.com/pdfs/e3872.pdf.
37. Olson R.W., Swope W.C. *J. Appl. Phys.*, **72**, 3686 (1992).
38. Lorazo P., Lewis L.J., Meunier M. *Phys. Rev. B*, **73**, 134108 (2006).
39. Amendola V., Meneghetti M. *Phys. Chem. Chem. Phys.*, **15**, 3027 (2013).
40. Yan Z., Chrisey D.B. *J. Photochem. Photobiol. C: Photochem. Rev.*, **13**, 204 (2012).
41. Sakamoto M., Fujistuka M., Majima T. *J. Photochem. Photobiol. C: Photochem. Rev.*, **10**, 33 (2009).
42. Olenin A.Yu., Lisichkin G.V. *Russ. Chem. Rev*., **80**, 605 (2011) [*Usp. Khim.*, **80**, 635 (2011)].
43. Kreibig U., Gartz M., Hilger A., Hövel H., Quinten M., Wagner D. in: *Functional Properties of Nanostructured Materials* (Ed. by R. Kassing et al.) (Dordrecht, Netherlands: Springer, 2005, p. 75).
44. Tsvetkov M.Yu., Bagratashvili V.N., Panchenko V.Ya., Rybaltovskiy A.O., Samoilovich M.I., Timofeev M.A. *Nanotechnol. Russ*., **6**, 619 (2011) [*Ross. Nanotekh.*, **6**, 109 (2011)].
45. Khlebtsov N.G., Dykman L.A. *J. Quantitat. Spectroscopy & Radiat. Transfer*, **111**, 1 (2010).
46. Zimmer K., Böhme R. *Laser Chem.*, Article ID 170632 (2008); doi:10.1155/2008/170632 (2008).
47. Simakin A.V., Loubnin E.N., Shafeev G.A. *Appl. Phys. A*, **69**, S267 (1999).
48. Simakin A.V., Lubnin E.N., Shafeev G.A. *Quantum Electron.*, **30**, 263 (2000) [*Kvantovaya Elektron.*, **30**, 263 (2000)].
49. Bloembergen N. *Appl. Opt.*, **12**, 661 (1973).
50. Skripov V.P., Sinitsyn E.N., Pavlov P.A., Ermakov G.V., Muratov G.N., Bulanov N.V., Baidakov V.G. *Teplofizicheskie svoistva zhidkostei v metastabil'nom sostoyanii* (Thermophysical Properties of Liquids in Metastable State. Reference Book) (Moscow: Atomizddat, 1980).
51. Martynyuk M.M. *Fazovye perekhody pri impul'snom nagreve* (Phase Transitions Under Pulsed Heating) (Moscow: UDN Press, 1999).
52. Zhigilei L.V., Garrison B.J. *Appl. Phys. A*, **69**, S75 (1999).
53. Miotello A., Kelly R. *Appl. Phys. A*, **69**, S67 (1999).
54. Bulgakova N.M., Bulgakov A.V. *Appl. Phys. A*, **73**, 199 (2001).
55. Song K.H., Xu X. *Appl. Surf. Sci.*, **127–129**, 111 (1998).
56. Tsibidis G.D., Barberoglou M., Loukakos P.A., Stratakis E., Fotakis C. *Phys. Rev. B*, **86**, 115316 (2012).
57. Ben-Yakar A., Harkin A., Ashmore J., Byer R.L., Stone H.A. *J. Phys. D: Appl. Phys.*, **40**, 1447 (2007).
58. Weingärtner H., Franck E.U. *Angew. Chem. Int. Ed.*, **44**, 2672 (2005).
59. Gorbatyi Yu.E. *Sverkhkrit. Flyuidy: Teor. Prakt.*, **2**, 40 (2007).
60. Ashkenasi D., Rosenfeld A., Varel H., Wähmer M., Campbell E.E.B. *Appl. Surf. Sci.*, **120**, 65 (1997).
61. Martynyuk M.M. *Fiz. Goreniya Vzryva*, **13**, 213 (1977).
62. Yang G.W. *Progr. Mater. Sci.*, **52**, 648 (2007).
63. Karásek P., Grym J., Roth M., Planeta J., Foret F. *Lab. Chip.*, **15**, 311 (2015).
64. Cansell F., Aymonier C. *J. Supercrit. Fluids*, **47**, 508 (2009).
65. Franjic K, Miller R.J.D. *Phys. Chem. Chem. Phys.*, **12**, 5225 (2010).
66. Pushkin V., Bychkov A.S., Karabutov A.A., Potemkin F.V. *Laser Phys. Lett.*, **15**, 065401 (2018).
67. Kuznetsova D. et al. *Biofabrication*, **9**, 025009 (2017).
68. Samiei E., Tabrizian M., Hoorfar M. *Lab. Chip.*, **16**, 2376 (2016).
69. Huang M., Zhao F., Cheng Y., Xu N., Xu Z. *Opt. Express*, **16**, 19354 (2008).